# Raw Defines a Distinct TIR-fold cADPR Hydrolase Family and Cooperates with dSarm in Development and Axon Degeneration

Feng **Chen**[1#], Zhuo **Chen**[1#], Yongjun **Tan**[2#], Xin Ye **Shen**[1,3], Matthew **Leong**[4], Jian Yuan **Yang**[1], Wan Hua **Li**[1], Yun Nan **Hou**[5], Guo **Bao**[1], Yue Jun **Chen**[1], Yu Ran **Ma**[1], Ting-Fung **Chan**[3], Hon Cheung **Lee**[5], Gyeong Hun **Baeg**[6], Dapeng **Zhang**[2,7*], Yong Juan **Zhao**[1,5*]

[1] Ciechanover Institute of Precision and Regenerative Medicine, School of Medicine, The Chinese University of Hong Kong, Shenzhen, China, 518172

[2] Department of Biology, College of Arts and Sciences, Saint Louis University, St. Louis, MO 63103, USA

[3] School of Life Sciences, The Chinese University of Hong Kong, HKSAR, China

[4] School of Medicine, Saint Louis University, St. Louis, MO 63103, USA

[5] State Key Laboratory of Chemical Oncogenomics, Key Laboratory of Chemical Genomics, Peking University Shenzhen Graduate School, Shenzhen, China, 518055

[6] Faculty of Health Sciences, University of Macau, Macau SAR, China

[7] Program of Bioinformatics and Computational Biology, Saint Louis University, St. Louis, MO 63103, USA

[#] Equal contribution

* Corresponding authors: dapeng.zhang@slu.edu; zhaoyongjuan@cuhk.edu.cn

Keywords: Raw/OLRN-1, cADPR, NAD, SARM1/dSarm, TIR domain, axon degeneration, development, evolutionary analysis

## Abstract

Conserved TIR domain proteins play essential roles in immune signaling, development, and neurodegeneration. Here, we identify Raw as a member of a distinct TIR protein family that functions as a cADPR-specific hydrolase, with catalytic mutations phenocopying delayed axon degeneration. While Raw and dSarm synergistically deplete NAD to drive axon degeneration, they antagonistically regulate cADPR levels in S2 cells, modulating development-related genes via the Ask1/JNK pathway, a non-canonical cADPR signaling mechanism independent of calcium mobilization. Consistently, Raw knockdown in fly wing discs elevates JNK phosphorylation, alters developmental gene expression, and causes wing defects, all rescued by Ask1 knockdown. Similarly, dSarm overexpression induces pupal lethality, which is also reversed by Ask1 suppression. Phylogenetic analysis reveals the co-evolution of dSarm and Raw across species, with conserved cADPR-hydrolysis activity observed in C. elegans Olrn-1. These findings underscore the distinct yet cooperative roles of dSarm and Raw in cADPR signaling-mediated development and NAD depletion-driven axon degeneration.

## Significance Statement

This research uncovers how two proteins, SARM1/dSarm and Raw, work together in tissue development and axon degeneration. Raw was found to have a unique activity in hydrolyzing a second messenger, cADPR. During axon degeneration, Raw collaborates with dSarm to degrade NAD; while in developmental stages, Raw terminates the cADPR signaling initiated by dSarm. The study also showed that in non-vertebrates, SARM1 and Raw evolved together, while vertebrates lost Raw, and SARM1 took over its functions. This discovery highlights the importance of the cADPR signaling pathway in development, providing new insights into cellular processes and potential implications for treating neurodegenerative diseases.

## Introduction

Toll/Interleukin-1 Receptor (TIR) domains are evolutionarily conserved signaling modules associated with innate immunity in both animals and plants, which were traditionally believed to mediate protein-protein interactions within various signaling pathways(1). Recently, research has expanded the functional repertoire of TIR-containing proteins beyond their scaffolding roles by unveiling intrinsic enzymatic activities across all three biological kingdoms(2). The majority of these enzymatically active TIR domains utilize nicotinamide adenine dinucleotide (NAD) as their substrate, exemplified by bacterial AbTir(3) and plant RPP1(4). Rare cases, such as plant RBA1, have been shown to utilize DNA and RNA as substrates(5). The enzymatic products derived from these reactions function as signaling molecules involved in diverse biological processes. For instance, bacterial TIR proteins generate N7-cADPR, which activates caspase-like proteins to induce cell death during phage infection(6), thereby positioning TIR domains as critical regulators of cellular metabolism and stress responses.

Sterile Alpha and TIR motif-containing 1 (SARM1), known as dSarm in *Drosophila melanogaster*, is the only enzymatically active TIR protein currently recognized in animal cells. It was identified through genetic screening for delayed axon degeneration (AxD) phenotypes(7). Studies proved that SARM1 executes AxD by enzymatically cleaving NAD(8). Specifically, SARM1 functions as a multifunctional NAD-consuming enzyme, in which the cyclization of NAD to cyclic ADP-ribose (cADPR)(8-10), hydrolysis of NAD to ADP-ribose (ADPR)(8, 10), and base-exchange conversion of NADP to nicotinic acid adenine dinucleotide phosphate (NAADP) under acidic conditions(10, 11) are alternative outcomes of the same catalytic mechanism. Upon axonal injury or cellular stress, SARM1 is activated by a decline in NAD levels(12) and the accumulation of nicotinamide mononucleotide (NMN)(10), leading to rapid NAD depletion within the axon. This depletion triggers a cascade of molecular events that culminate in axonal disintegration and fragmentation(13). The identification of SARM1 as a pivotal regulator of AxD has opened new avenues for developing therapeutic

strategies(14-16) aimed at inhibiting its activity to preserve axonal integrity in neurodegenerative disorders.

Beyond SARM1, other proteins have also been implicated in regulating axon degeneration and maintaining neuronal health, among which Raw is of particular interest. Loss-of-function mutations in Raw result in a delayed AxD phenotype similar to that observed in dSarm mutants(17). Further studies have revealed that Raw has synergistic effect with dSarm in promoting axon degeneration, however, they exhibit opposing roles in regulating the growth of neuromuscular junctions through the JNK pathway(18). Additionally, Raw mutants show various developmental defects in embryonic dorsal closure(19), glial development(20), intestinal regeneration(21), and etc. The mechanisms underlying this differential regulation remain unclear.

Through comparative genomics analysis and AlphaFold structural predictions(22), we found that Raw contains two TIR domains, suggesting its potential involvement in NAD metabolism. In this study, we documented that Raw does not target NAD, but is a highly efficient and specific enzyme for hydrolyzing cADPR. We then showed that Raw acts synergistically with dSarm to consume NAD, which leads to axon degeneration. During development, the two enzymes, however, work oppositely to regulate cADPR levels, which, in turn, modulate the cADPR-dependent Ask1/JNK-signaling pathway. This work reinforces the emerging paradigm of TIR proteins as versatile signaling enzymes, whose catalytic outputs are dynamically tuned to meet cellular demands.

## Results

### Raw defines a novel family of TIR domain proteins.

To elucidate the biological function of Raw, we first dissected its domain architecture using detailed sequence/profile and structural analyses. This revealed that Raw consists of four globular domains, including two dimerization domains (DD1 and DD2) and two TIR domains (TIR-1 and TIR-2) (**Fig. 1A-B; Supplementary Fig. S1**). Examination of conservation patterns among all retrieved Raw homologs at the NCBI

database identified distinct sets of conserved residues in TIR-1 (Phe354, Cys359, Glu396, and Glu422) and TIR-2 (Asp946, Arg949, Tyr953, and Asp956) (**Supplementary Fig. S2-3**). Importantly, the AlphaFold models predict the four structured domains of Raw (excluding disordered loops) with high confidence, providing a reliable framework to examine the structural context of these conserved residues. By integrating sequence/profile-based conservation analyses with structural mapping, we found that the conserved residues cluster together to form a putative catalytic pocket, suggesting that they are under strong functional selection and that the dimeric assembly of both TIR domains is essential for Raw activity (**Fig. 1B, Supplementary Fig. S2-3**). In addition, disordered loops were observed within the DD2 and TIR-2 domains as well as in the inter-domain regions (**Supplementary Fig. S1A**). These loops are present only in a subset of Raw homologs and show no conserved residues, suggesting that they are unlikely to be catalytically or functionally critical.

To further clarify evolutionary relationship of Raw TIR domains, we compiled representative sequences from all known eukaryotic TIR domain families, including animal Toll-like receptor (TLR)(23), plant nucleotide-binding leucine-rich repeat receptors (NLRs)(4), animal SARM1(8), animal Similar Expression to Fibroblast Growth Factor (SEF) proteins(24), and various bacterial TIR versions that we identified in many anti-phage systems(25), and combined them with Raw TIR sequences. Sequence similarity-based network clustering revealed that Raw TIR domains and their bacterial homologs form a distinct cluster, separate from other known TIR families (**Fig. 1C**). Subsequent phylogenetic analysis further supports that Raw TIR domains, and their bacterial homologs constitute previously unrecognized family of the TIR domain proteins (**Fig. 1D**).

**Raw displays a specific cADPR hydrolyzing activity.**

Since TIR domains in SARM1(8), plant NLRs(4) and bacterial TIRs(3) have been found to possess enzymatic activities utilizing NAD as a substrate, and Raw mutants showed the AxD delay phenotype, we hypothesized that Raw might also exhibit similar

enzymatic activities. To investigate this possibility, we constructed an expression vector encoding a full-length Raw with an N-terminal Flag tag and overexpressed it in *Drosophila* Schneider 2 (S2) cells, the most commonly used *Drosophila* cell line derived from a primary culture of late stage (20-24 hours old) embryos(26). Lysates were first analyzed by Western blot to confirm the correct expression of the tagged Raw protein (**Fig. 2A**), followed by an activity measurement using a cycling assay(27). Contrary to the initial expectations, lysates from S2 cells overexpressing Raw did not induce any significant changes in NAD levels (**Fig. 2B**, lower panel; different NAD concentrations were tested, shown in **Supplementary Fig. S4A**). Instead, these lysates markedly reduced cADPR levels compared to control lysates (**Fig. 2B**, upper panel). These findings suggest that Raw may possess a distinct enzymatic activity that utilizes cADPR as its substrate.

To further characterize the enzymatic reaction, we expressed Raw with an Maltose bind protein (MBP) tag in *E.coli* and purified the protein by a maltose affinity column (SDS-PAGE analysis see in **Supplementary Fig. S4B**). Activity measurements confirmed that the semi-purified Raw protein could decrease cADPR levels, as assessed by the cycling assay, with BSA serving as a negative control (**Fig. 2C**). High-performance liquid chromatography (HPLC) analysis of the reaction products revealed that, concomitant with the decrease in cADPR, ADPR was progressively produced over the course of the reaction (**Fig. 2D**; MS confirmation of the reactants is shown in **Supplementary Fig. S4C**). In contrast, Raw was unable to hydrolyze the two fluorescent analogs of cADPR, cyclic GDP ribose (cGDPR, **Supplementary Fig. S4D**) and cyclic IDP ribose (cIDPR, **Supplementary Fig. S4E**), suggesting the high substrate specificity of Raw. Thus, we conclude that Raw catalyzes the hydrolysis of cADPR, as depicted in the reaction equation in **Figure 2E**. We further characterized the Michaelis-Menten kinetics of Raw using the cycling assay. Nonlinear regression based on the Michaelis-Menten model yielded $K_m$ and $k_{cat}/K_m$ values of 47.36 nM and 2.75 x $10^7$ $M^{-1}s^{-1}$, respectively (**Fig. 2F**), which were further validated by the Lineweaver-Burk plot (**Supplementary Fig. S4F**). These results suggest that Raw is

a highly efficient and specific enzyme for hydrolyzing cADPR. This is a remarkable finding, as since the discovery of cADPR in 1989(28, 29), SARM1 and CD38 have been the only known enzymes that can hydrolyze it, but with much higher $K_m$ and lesser specificity. Also distinct is that Raw does not hydrolyze NAD. It thus appears that Raw is uniquely specific to cADPR.

To validate Raw's enzymatic activity in cells, we synthesized double-stranded RNAs (dsRNAs) *in vitro* targeting different regions of *Raw* mRNA and transfected into S2 cells. After incubation with the cells, Raw expression levels were quantified by qRT-PCR, and cellular cADPR levels were measured using the cycling assay. Three different antisense sequences exhibited varying knockdown efficiency, with sequence #1 achieving the highest and sequence #3 the lowest (**Fig. 2G**). An inverse correlation between cADPR levels and Raw expression levels was observed (**Fig. 2G**), consistent with the enzymatic activity of Raw. Furthermore, lysates from wildtype S2 cells demonstrated efficient degradation of cADPR, whereas Raw knockdown nearly abolished this activity (**Fig. 2H**), indicating that Raw is endogenously expressed and constitutively active in S2 cells.

Finally, we assessed Raw's activity *in vivo*. We crossed flies carrying UAS-Raw RNAi (RNA interference; VDRC#101255) or UAS-Raw OE (overexpression)(17) constructs with virgin flies carrying *elav*-Gal4, a pan-neuronal driver, to generate flies with neuronal knockdown and over-expression of Raw, respectively. Head tissues were collected from 2-week-old F1 adult flies and subjected to the cycling assay to measure cADPR levels in the brain. The results revealed significantly elevated cADPR levels in Raw knockdown flies and reduced levels in Raw OE flies (**Fig. 2I**), consistent with our *in vitro* and *in cellulo* findings.

**Enzymatic activities of Raw mutants correlate to AxD delay phenotypes.**

Next, we investigated the roles of the two TIR domains and several key residues in Raw's enzymatic activity. To determine whether the TIR domains are essential for Raw's function, we generated various constructs encoding truncated forms of Raw with a Flag-tag (**Fig. 3A**). Lysates from cells transfected with these constructs were

analyzed by Western blots (**Supplementary Fig. S5A**) and incubated with cADPR *in vitro*, with residual cADPR levels quantified using the cycling assay. As shown in **Fig. 3B**, both TIR1 and TIR2 domains are required for enzymatic activity, as deletion of either domain resulted in complete loss of function (compare TIR1, TIR2, ΔTIR1 and ΔTIR2 with full-length Raw). The ΔN truncation, which removes the DD1-containing N-terminal region of Raw, retained partial enzymatic activity, although significantly reduced, suggesting DD1 is important for full activity but not strictly required. Further removal of DD2, in the sample containing both TIR1 and TIR2, did not restore the activity of ΔN, indicating that DD2 is indispensable for Raw's enzymatic function.

Several Raw mutants, including $raw^{dcp\text{-}1}$, $raw^{155.27}$, and $raw^{134.47}$, exhibit delayed AxD following injury(17). They correspond to the mutants A532D, R949C, and Y953N, respectively. Ala532 is located at the interface between DD2 and TIR2, while Arg949 and Tyr953 are situated at the TIR1-TIR2 interface (**Fig. 1B**). We generated these point mutants and confirmed that they were expressed at levels comparable to wildtype (WT) Raw. However, these mutants lost their cADPR hydrolase activity, with A532D retaining only a minimal level of activity, while R949C or Y953N showing complete loss of function (**Fig. 3C**). Using the same expression and purification protocol as in **Fig. 2F**, we purified Y953N and performed *in vitro* activity assays (**Supplementary Fig. S5B**), which revealed no detectable activity (**Supplementary Fig. S5C**).

To further validate the impact of these mutations, we measured cADPR levels in the brain tissues of $raw^{dcp\text{-}1}$ mutants, which were significantly elevated compared to WT (**Fig. 3D**). Additionally, homogenates from $raw^{dcp\text{-}1}$ brain tissues demonstrated reduced cADPR hydrolyzing activity *in vitro* (**Fig. 3E**). Collectively, these mutations result in correlated loss in both enzymatic activity and AxD phenotype (**Fig. 3F**), suggesting that cADPR hydrolysis by Raw is critical for axon degeneration.

Comparative structural analysis between Raw and other known cADPR-metabolizing enzymes, including SARM1(12), CD38(30) and ADP-ribosyl cyclase(31), revealed a putative catalytic pocket between the two TIR domains. Similar to these enzymes, Raw contains two conserved glutamic acid residues within this pocket,

identified as potential catalytic residues (**Supplementary Fig. S6A**). AlphaFold3(32) modeling of the Raw/cADPR complex (**Supplementary Fig. S6B**) confirmed that cADPR binds within this pocket, with the “northern ribose” contacting E396 and E422, and the pyrophosphate group interacting with R949 (**Fig. 3G**). As with the R949C mutant (**Fig. 3C**), substitution of either glutamate abolished cADPR-hydrolyzing activity without affecting protein expression (**Fig. 3H**), supporting that the conclusion that E396 and E422 form the catalytic center.

Based on these findings, we propose two catalytic mechanisms. In the first, consistent with classical paradigm, E422 forms fork-like hydrogen bonds with the 2’ and 3’ hydroxyl groups of the northern ribose, while E396 activates a water molecule to attack the anomeric carbon, generating ADPR (**Supplementary Fig. S6C**). In the second, more aligned with the AlphaFold3 structure, E422 hydrogen-bonds to the 3’ hydroxyl group, while E396 engages the 2’ hydroxyl and jointly attacks the anomeric carbon to form a covalent intermediate; a water molecule then cleaves this bond to release ADPR (**Supplementary Fig. S6D**). The models remain hypothetical and will require further biochemical and structural studies to validate their accuracy.

**Raw cooperates with dSarm in consuming NAD.**

Since NAD depletion is a key trigger for AxD, we next investigated whether Raw synergistically promotes NAD consumption by dSarm. We first prepared recombinant dSarm and hSARM1(33) using mammalian cell expression systems and purified them via Strep-Tactin affinity chromatography (**Supplementary Fig. S7A**). Recombinant dSarm, hSARM1, or Raw each was incubated with NAD, and the resultant products were analyzed by HPLC. The results confirmed that Raw does not utilize NAD as a substrate (**Fig. 4A**, red). dSarm primarily produced cADPR (**Fig. 4A**, blue), while hSARM1 predominantly generated ADPR (**Fig. 4A**, purple), consistent with previous characterizations of their TIR domains(8). The quantification revealed that 74% of dSarm’s products were cADPR, whereas 95% of hSARM1’s products were ADPR (**Fig. 4B**), suggesting that dSarm functions mainly as a cyclase, cyclizing NAD to cADPR, whereas SARM1 acts primarily as a NAD hydrolase.

To investigate the role of Raw in neurodegeneration, we hypothesized that dSarm and Raw together may synergistically convert NAD to cADPR and sequentially hydrolyze it to ADPR, thereby promoting NAD degradation. To test this hypothesis, we incubated NAD with both dSarm and Raw. Indeed, the presence of Raw accelerated NAD depletion significantly compared to incubation with dSarm alone and resulted in a lower steady equilibrium level of NAD (**Fig. 4C**; similar results were obtained for 100 μM NAD, shown in **Supplementary Fig. S7B**). Notably, Raw did not consume NAD by itself. The fact that the steady NAD level reached with dSarm alone was higher than with Raw as well suggests that cADPR produced may exert product inhibition on dSarm. Consistently, in the presence of cADPR, NAD consumption was significantly slowed down (**Fig. 4D**; similar results were obtained for 100 μM NAD, shown in **Supplementary Fig. S7C**). The extent of inhibition was similar to that observed with dSarm-TIR, the TIR domain of dSarm (**Supplementary Fig. S7D**), confirming product inhibition by cADPR.

To further validate the synergistic effect of dSarm and Raw in cells, we transfected S2 cells with the indicated expression vectors and confirmed protein expression via Western blotting (**Supplementary Fig. S7E**). Cellular levels of cADPR and NAD were measured by the cycling assay. Overexpression of dSarm significantly elevated cADPR levels, which were completely reversed by co-expression of Raw (**Fig. 4E**). Expression of dSarm alone did not alter cellular NAD levels, likely due to robust NAD synthesis in S2 cells. However, co-expression of Raw with dSarm led to a significant decrease in NAD levels (**Fig. 4F**), supporting the synergistic role of dSarm and Raw in NAD depletion.

We further validated these effects in *ex vivo* assays. Brain tissues were treated with CZ-48, a cell-permeant NMN mimic and activator of hSARM1(10), which significantly elevated cADPR levels in both WT and $raw^{dcp\text{-}1}$ mutant flies (**Fig. 4G**). Notably. mutants exhibited a much higher elevation. These results suggested that dSarm can be activated by CZ-48, consistent with the fact that dSarm is also activated by NMN. In the NAD assay, we found that CZ-48 treatment also decreased NAD levels

in WT flies but not in *raw*$^{dcp-1}$ mutants, and the basal NAD levels of the mutants were significantly higher than those of WT (**Fig. 4H**), further indicating dSarm and Raw collaboratively contribute to NAD reduction.

To determine whether Raw and dSarm are co-expressed in neurons, we analyzed their expression profiles in single cells from the *Drosophila* head using tSNE plots, as described in Methods. Green signals represent dSarm expression, red signals indicate Raw expression, and yellow signals denote co-expression of both proteins (**Supplementary Fig. S7F**). Based on cell type annotations (**Supplementary Fig. S7G**), dSarm is expressed in neurons, glia cells, epithelial cells, muscle cells, etc, while Raw is expressed in epithelial cells, sensory neurons, pigment cells, unannotated cells, etc. Notably, they are co-expressed in neurons, supporting their collaborative function in AxD. Intriguingly, the highest level of co-expression was observed in epithelial cells, suggesting a potential role in epithelial functions such as organ development, which will be discussed in the subsequent sections.

Based on our biochemical findings and the previously observed AxD delay phenotype in dSarm or Raw mutants, we propose a working model for the roles of dSarm and Raw in AxD (**Fig. 4I**). In healthy WT axons, basal NAD levels are maintained at high levels. Upon injury, dSarm is activated and catalyzes the cyclization of NAD into cADPR. Raw subsequently hydrolyzes cADPR, leading to NAD depletion and ultimately axon degeneration. In dSarm mutants, the initial reaction is blocked, preventing NAD depletion and AxD. In Raw mutants, the secondary reaction is blocked, causing accumulation of cADPR, which then inhibits dSarm, thereby also preventing NAD depletion and AxD. We believe that this model effectively explains the enzymatic interplay between dSarm and Raw in regulating NAD levels and axon degeneration.

**cADPR activates Ask1/JNK pathway correlating with organ development.**

To elucidate the roles of dSarm and Raw in developmental processes, we focused on the Ask1/JNK pathway(34, 35), which has been known to be regulated by Raw(17, 36) or dSarm(37, 38). As shown above, dSarm produces cADPR while Raw hydrolyzes it, we thus investigated the possibility that cADPR may act as a mediator of

developmental processes through regulating the Ask1/JNK signaling pathway. We transfected S2 cells, an ideal embryonic cell model for studying development, with vectors to either overexpress dSarm (dSarm-OE) or knockdown Raw (Raw-RNAi), thereby elevating cADPR levels. We then assessed whether these manipulations could induce the expression of downstream genes of the Ask1/JNK pathway such as *Matrix metalloproteinases 1* (*Mmp1*)(39).

Expression analyses confirmed successful overexpression of dSarm in dSarm-OE cells and effective knockdown of Raw in Raw-RNAi cells (**Supplementary Fig. S8A**). Nucleotide measurements revealed that dSarm-OE and Raw-RNAi had minimal effects on NAD (**Fig. 5A**, lower panel), whereas both manipulations significantly elevated cADPR levels (**Fig. 5A**, upper panel). Concurrently, we measured the expression of Mmp1, transcriptionally regulated by the JNK pathway(39). Both dSarm-OE and Raw-RNAi upregulated Mmp1 expression, although the increase induced by Raw-RNAi was less pronounced (**Fig. 5B**). This trend correlates closely with the observed cADPR levels in these cell lines (**Fig. 5A**), supporting the notion that cADPR, rather than NAD, serves as the signaling molecule that activates the JNK pathway.

To obtain direct evidence that cADPR can activate the JNK pathway, we treated S2 cells with the cell-permeant cADPR analog, 8-Br-cADPR. The 8-bromo substitution at the 8-position of cADPR has been widely used to antagonize cADPR's calcium-releasing activity in sea urchin homogenate(40) or mammalian systems(41), though its function in *Drosophila* cells remains unclear. Treatment with 8-Br-cADPR significantly increased Mmp1 expression, whereas the control compound, 8-Br-ADPR (an analog of ADPR, linear form of 8Br-cADPR), had no such effect (**Fig. 5C**). These results indicate that 8-Br-cADPR functions as a cADPR mimics to activate the JNK pathway, thereby supporting our hypothesis.

To explore cADPR signaling at the transcriptomic level, we treated S2 cells with 8-Br-cADPR and 8-Br-ADPR and performed bulk RNA sequencing. Following data processing and quality control, principal component analysis (PCA) was performed to reduce the dimensionality of the dataset and identify key sources of variation (**Fig. 5D**).

The first principal component (PC1) accounted for 80.38% of the variance and separated the 8-Br-cADPR-treated samples from controls, while the second principal component (PC2) accounted for 10.88% and minimally distinguished vehicle from 8-Br-ADPR-treated samples. This indicates that the alteration in gene expression profiles is dependent on the cyclic structure of cADPR.

Differential gene expression analysis identified 251 upregulated and 97 downregulated RNAs in 8-Br-cADPR-treated cells compared to the 8-Br-ADPR control (**Fig. 5E** and **Supplementary Table S1**). A heatmap of these differentially expressed genes confirmed the clustering observed in the PCA and illustrated the expression changes for each gene (**Fig. 5F**). We validated the expression of several genes, including *Puchered* (*Puc*), *Slowdown* (*Slow*), *CG15347*, *Diptericin B* (*DptB*), *Galactose-1-phosphate uridylyltransferase* (*Galt*), and *Peptidoglycan Recognition Protein SB 1* (*PGRP-SB1*), in 8-Br-cADPR-, 8-Br-ADPR- or vehicle-treated cells using qRT-PCR (**Fig. 5G**). Additionally, similar expression changes were observed in dSarm-OE and Raw-RNAi cells (**Supplementary Fig. S8B**), further suggesting that the gene expression is regulated by cADPR signaling and that 8-Br-cADPR effectively mimics this signal.

To identify cADPR-regulated gene sets, gene set enrichment analysis (GSEA) was conducted by comparing the RNAseq data from cells treated with 8-Br-cADPR or 8-Br-ADPR. Using the GO gene set collection, we found that cells treated with 8-Br-cADPR exhibited significant upregulation of transcripts encoding proteins involved in organ development (**Fig. 5H** and **Supplementary Table S2**), which aligns with the developmental changes observed in Raw mutants(36, 42-44). Conversely, transcripts downregulated by 8-Br-cADPR treatment were associated with bacterial defense responses and metabolism (**Supplementary Fig. S8C**), suggesting potential novel functions of cADPR in these pathways as well and be investigated in later studies. Furthermore, GSEA revealed a significant enrichment of the “MAPK signaling pathway” (NES = 1.407, FDR = 0.089) (**Supplementary Fig. S8D**) in 8-Br-cADPR-treated cells

compared to vehicle-treated cells, supporting the role of cADPR in activating the Ask1/JNK pathway, either directly or indirectly.

**Raw and dSarm have opposing roles in regulating cADPR/Ask1/JNK pathway during development.**

Given that cADPR signaling is significantly correlated with organ development (**Fig. 5H**) and that both Raw and dSarm are co-expressed highly in epithelial cells (**Supplementary Fig. S7F-G**), we employed the *Drosophila* wing model as indicator to investigate the role of the dSarm/cADPR/Raw pathway. Single-cell gene expression analysis revealed that both dSarm and Raw are expressed within the wing imaginal disc (**Supplementary Fig. S8E**). Additionally, Raw was found to co-express with several segment polarity genes, including *cubitus interruptus* (*Ci*), *Mirror* (*Mirr*), *Decapentaplegic* (*Dpp*), *Patched* (*Ptc*), *Hedgehog* (*Hh*), and *Scalloped* (*Sd*), in varying degrees (**Supplementary Fig. S8F**), providing information about its relative spatial expression.

To elevate cADPR levels in the entire wing imaginal disc, *raw*-RNAi was overexpressed under the control of *Sd*-Gal4. The F1 progeny developed normally overall; however, they exhibited severely malformed wings (**Fig. 6A**; the quantitative results in **Fig. 6B**), indicating that excessive cADPR impairs wing development. To further elucidate the pathway, we double-knockdown *raw* and *ask1*, encoding a kinase upstream of the JNK pathway implicated in dSarm functions(37, 38), under control of the same driver, *Sd*-Gal4. Notably, the wing defects were substantially rescued in the flies lacking both *raw* and *ask1* (**Fig. 6A-B**), suggesting that Ask1 acts downstream of Raw in animal development.

We dissected imaginal wing discs out of third-instar larvae and performed Western blotting and gene expression analyses. Knockdown of *raw* resulted in the phosphorylation of JNK (**Fig. 6C**) and an elevated expression of a subset of genes, including *Puc* and *slowdown* (*Slow*) (**Fig. 6D**), which have been shown to be elevated by cADPR in S2 cells (**Fig 5**). Furthermore, JNK phosphorylation and the induction of

these genes was noticeably attenuated by simultaneous knockdown of Ask1 (**Fig. 6C-D**), reinforcing the conclusion that Ask1/JNK functions downstream of cADPR.

Similarly, *dSarm* was ectopically expressed using the *Sd*-Gal4 driver to elevate cADPR in wing discs. *dSarm*-OE flies failed to pupate on Day 9, and this defect was partially rescued by *ask1* knockdown (**Fig. 6E-F**), The *ask1* knockdown group contained fewer animals, suggesting an early developmental role for Ask1, and RNAi #1 showed limited rescue, likely due to variable residual expression. Together with previous reports(37, 38), these data support the model in which dSarm and Ask1 operate within the cADPR signaling pathway.

The phenotypic difference between *Sd>raw*-RNAi and *Sd>dSarm*-OE is likely due to difference in the expression pattern, amounts of these two enzymes and the extents of cADPR elevation. *Sd* has been reported to be expressed in a variety of cells, which may not be restricted in wing development, such as the central and peripheral nervous system and the musculature during development(45). The accumulation of cADPR in them may cause the observed developmental arrest in *Sd>dSarm*-OE flies. Alternatively, Raw and dSarm may have other different functions in addition to their enzymatic activities, a possibility cannot be excluded.

**Co-evolution of Raw and SARM1**

To summarize our findings, we propose that dSarm and Raw cooperate to deplete NAD by dSarm converting NAD to cADPR and subsequently Raw hydrolyzing cADPR to ADPR, leading to AxD (**Fig. 7A**, left). In contrast, during development dSarm and Raw oppositely regulate cADPR levels, with dSarm synthesizing and Raw degrading cADPR to control wing formation and pupae development through the Ask1/JNK pathway (**Fig. 7A**, right).

Building on the evidence of the molecular interaction between Raw and SARM1, we investigated whether their evolutionary histories are interconnected. Phylogenetic analyses of their TIR domains revealed a notable convergence in their evolutionary trajectories (**Fig. 7B**). Both Raw TIR and SARM1 TIR domains appear to have originated from bacterial homologs introduced into eukaryotic lineages via horizontal

gene transfers. These domains are widely distributed across diverse eukaryotes, including nematodes and multiple major invertebrate phyla such as mollusks and arthropods. A key divergence is observed in vertebrates, where SARM1 remains conserved while Raw is absent. This distribution pattern correlates with distinct biochemical capabilities of SARM1 between invertebrates and vertebrates (**Fig. 4A-B**). In vertebrates, SARM1 mainly cleaves NAD into ADPR, mostly functioning as a fully autonomous NADase. In contrast, invertebrate SARM1 primarily generates cADPR from NAD, necessitating further enzymatic processing by Raw to complete the NADase function, with both proteins oppositely regulating cADPR signaling. The complementary presence and cooperation of SARM1 and Raw in invertebrates versus the singular functionality of SARM1 in vertebrates, highlight a case of co-evolution. Furthermore, these findings suggest that the phyletic pattern and enzymatic interdependence observed for SARM1 and Raw reflect evolutionary adaptations that enabled vertebrate SARM1 to act independently, ultimately leading to the loss of Raw in vertebrate lineages.

In the course of phylogenetic analysis, we discovered that TIR-1 and Olrn-1 are the *Caenorhabditis elegans* homologs of dSarm and Raw, respectively. TIR-1 has been extensively studied for its NADase activity and role in axon degeneration(46), whereas Olrn-1 has been reported to be functioned in the development of olfactory neurons(47).

Here, we tested the activity of Olrn-1 using the same experimental setup in **Figures 4E-F**. By overexpressing dSarm and Olrn-1 in HEK-293T cells (**Supplementary Fig. S9**), Olrn-1 successfully degraded the very high levels of cADPR produced by dSarm to the basal level. The combined action of Olrn-1 and dSarm also decreased the NAD levels significantly (**Fig. 7C**). This confirms the cADPR-degrading activity of Olrn-1 is as effective as Raw. In view of the central role of cADPR in *Drosophila* development shown in this study, it is likely that cADPR is also the regulating messenger in the development of *C. elegans*.

## Discussion

Prior to this study, traditional genetic approaches had established the roles of dSarm, Raw, and Ask1/JNK in both developmental processes and axon degeneration (AxD) in *Drosophila melanogaster(17, 18, 37, 38)*. However, the absence of a clear biochemical characterization of Raw hindered the development of a coherent working model that integrates these components. Our research addresses this gap by elucidating Raw's biochemical function as a cADPR-hydrolyzing enzyme. Through structural analysis and biochemical assays, we demonstrated that dSarm converts NAD to cADPR, while Raw subsequently hydrolyzes cADPR to ADPR. The combined action effectively depletes NAD, leading to AxD. In development, the two enzymes work oppositely, with Raw reducing while dSarm raising cADPR, which in turn activates the Ask1/JNK pathway. This integrated model establishes the pivotal role of cADPR and clarifies how these proteins orchestrate distinct signaling in cellular degeneration and development.

The discovery of cADPR's role in activating the Ask1/JNK kinase pathway in this study is a major advancement, greatly extending the repertoire of cADPR-signaling beyond its established function in calcium release from endoplasmic reticulum marks a significant advancement in the field. Since its identification in 1989 as a calcium-releasing agent(9), cADPR has been recognized as a crucial calcium messenger across diverse biological kingdoms(48). In our study, the use of 8-Br-cADPR, a cell-permeant analog of cADPR known to antagonize its calcium-releasing activity in sea urchin homogenate(40) or mammalian systems(41), revealed that 8-Br-cADPR can also act as an agonist, substituting cADPR to activate the Ask1/JNK pathway. This finding suggests that the receptor for cADPR in this case, possibly Ask1 itself, is different from that in calcium release process.

Findings in this study also highlight the prominence of cADPR signaling in *Drosophila*, not only in AxD and development (**Fig. 5**) but may also in metabolism and bacterial defense (**Supplementary Fig S8C**). Downstream pathways involved likewise may not be only limited to Ask1/JNK. Calcium signaling is another possibility that remains to be investigated. Our phylogenetic (**Fig. 7B**) also points to *C. elegans* as

another organism that cADPR-signaling may be equally prominent. That Olrn-1, an important mediator of the development of olfactory neurons, functions similar to Raw (**Fig. 7C**), is an obvious clue. A new frontier of investigation is ushered in.

In vertebrates, Raw is absent, but its function appears to be incorporated evolutionarily in SARM1 and CD38, both are capable of not only synthesizing cADPR from NAD but also hydrolyzing it to ADPR. Consequently, both behave like an NADase, functionally equivalent to combining dSarm and Raw. This raises an intriguing possibility that the cADPR synthesizing and hydrolyzing activities of SARM1 could be separately regulated to effect control of cADPR-signaling in vertebrates. Last but not least, the remarkable specificity of Raw for cADPR and not targeting NAD, makes it a valuable tool for manipulating cADPR levels in cells. In fact, we showed in this study that both Raw and Olrn-1 can be functionally expressed in mammalian cells, setting the stage.

The discovery of the TIR-containing Raw's enzymatic function exemplifies the power of combining comparative genomics and advanced structural prediction tools like AlphaFold(22) to annotate proteins of unknown function. This and other recent studies using these approaches have acuminated in a paradigm shift for the TIR proteins toward being signaling enzymes. The focus is now on cADPR and its isomers produced by the TIR proteins. Eukaryotic TIR proteins, such as dSarm and SARM1, cyclize NAD at the N1 position of the adenine ring to produce cADPR(10), which functions are described in this study. Plant and prokaryotic TIR proteins can cyclize NAD at other sites, such as N7 position of adenine, 2' or 3' position of the ribose to produce different isomers of cADPR, N7-cADPR, 2'-cADPR and 3'-cADPR, respectively. These isomers are found to regulate bacterial and plant immunity(6, 49-52). How these cADPR-messengers are removed after completing signaling is largely unknown. This study documents Raw is highly efficient and specific for degrading cADPR and is crucial in *Drosophila* development, emphasizing the fact that messenger removal system is also an important part of the cADPR-signaling pathway.

The remarkable prominence of cADPR in regulating *Drosophila* physiology shown

here is intriguing and unexpected. The same may also be true in *C. elegans* as suggested by the enzymatic similarity between Raw and Olrn-1 shown here. As genomic data expands and structural bioinformatics techniques advance, novel TIR-domain enzymes with unique substrate specificities will continue to be identified, further enriching our understanding of their roles in cellular physiology and evolution.

## Materials and Methods

For complete Materials and Methods, see the *SI_Materials and Methods.*

### Measurement of *in vitro* enzymatic activity

The pre-cleaned and adjusted protein lysate (working concentration: 50 μg/mL) or purified recombinant Raw protein (working concentration: ~0.5 μg/mL) was added to a reaction mixture containing 1 μM cADPR or NAD in PBS buffer. The reaction was carried out at room temperature for the specified time periods. To terminate the reaction, the mixture was filtered through a 0.22 μm PVDF membrane (Multiscreen 96-well Plate, hydrophobic PVDF membrane, MSIPS4510, Millipore) to remove the enzymes. Residual cADPR or NAD in the filtrate was quantified using a previously described cycling assay(27).

HPLC was used to analyze nucleotides. After terminating the reactions by filtration as described above, the reaction mixtures were loaded onto an AGMP-1 column connected to an HPLC system (Agilent 1260) equipped with an $OD_{260}$ detector. Separation of NAD, cADPR, and ADPR was achieved using a gradient elution of 100 mM TFA from 1% to 45%.

## Data, Materials, and Software Availability

RNA sequencing data have been deposited at BioProject (https://www.ncbi.nlm.nih.gov/bioproject/) under accession codes PRJNA1230788. The structural model of the Raw/cADPR complex is available in ModelArchive(53) (modelarchive.org) under the accession codes ma-onjq7.

## Acknowledgements

We thank Prof. Catherine Collins (Case Western Reserve University), Prof. Wenzhe Li (Tongji University) and Prof. Zizhang Zhou (Shandong Agricultural University) for providing fly lines, Prof. Hongli Hu and Dr. Qi Pan for their attempts in resolving the Cryo-EM structure of Raw, Prof. Yongfei Wang for suggestions in RNAseq data presentation, and Mr. Yezhou Liu for assistance with AlphaFold3 usage. This study was supported by National Natural Science Foundation of China (32470755), Shenzhen Science and Technology Innovation Committee (JCYJ20220818103009018), Shenzhen-Hong Kong Institute of Brain Science-Shenzhen Fundamental Research Institutions (2019SHIBS0004) and the 1+1+1 CUHK-CUHK(SZ)-GDST Joint Collaboration Fund (2025A0505000042). D.Z., Y.T., and M.L. are supported by funds from Saint Louis University. We would like to thank Sumyu Yang for drawing the illustration diagram. We thank ChatGPT-4o and DeepSeek for editing the grammar.

**Author contributions**

F.C. and Z.C. performed all the experiments presented in Fig. 2-4 and Fig. 5-7, respectively and prepared figures, and wrote the Methods section. Y.T. performed comparative genomics, phylogenetics, structural analysis and prepared figures. X.Y.S. performed all the analysis of RNAseq data. M.L. initiated the bioinformatics studies of Raw. J.Y.Y, W.H.L, Y.N.H., G.B., Y.J.C. assisted the experiments and structural analysis in Fig. 2-7. T.C., H.C.L., G.H.B. guided RNAseq analysis, cADPR studies and fly experiments, respectively and revised the manuscript. D.Z. guided the bioinformatics analysis, prepared figures, and assisted with manuscript writing. Y.J.Z. guided experimental design, prepared figures, and wrote the manuscript.

**Competing interests**

The authors declare no competing interest.

**Supporting information**

Supporting information includes “Supplemental information” file and three excel tables.

## Reference


1. S. Nimma *et al.*, Structural Evolution of TIR-Domain Signalosomes. *Front Immunol* **12**, 784484 (2021).
2. K. Essuman, J. Milbrandt, J. L. Dangl, M. T. Nishimura, Shared TIR enzymatic functions regulate cell death and immunity across the tree of life. *Science* **377**, eabo0001 (2022).
3. D. Ka, H. Oh, E. Park, J. H. Kim, E. Bae, Structural and functional evidence of bacterial antiphage protection by Thoeris defense system via NAD(+) degradation. *Nat Commun* **11**, 2816 (2020).
4. S. Ma *et al.*, Direct pathogen-induced assembly of an NLR immune receptor complex to form a holoenzyme. *Science* **370** (2020).
5. D. Yu *et al.*, TIR domains of plant immune receptors are 2',3'-cAMP/cGMP synthetases mediating cell death. *Cell* **185**, 2370-2386 e2318 (2022).
6. F. Rousset *et al.*, TIR signaling activates caspase-like immunity in bacteria. *Science* **387**, 510-516 (2025).
7. J. M. Osterloh *et al.*, dSarm/Sarm1 is required for activation of an injury-induced axon death pathway. *Science* **337**, 481-484 (2012).
8. K. Essuman *et al.*, The SARM1 Toll/Interleukin-1 Receptor Domain Possesses Intrinsic NAD(+) Cleavage Activity that Promotes Pathological Axonal Degeneration. *Neuron* **93**, 1334-1343 e1335 (2017).
9. H. C. Lee, T. F. Walseth, G. T. Bratt, R. N. Hayes, D. L. Clapper, Structural determination of a cyclic metabolite of NAD+ with intracellular Ca2+-mobilizing activity. *J Biol Chem* **264**, 1608-1615 (1989).
10. Z. Y. Zhao *et al.*, A Cell-Permeant Mimetic of NMN Activates SARM1 to Produce Cyclic ADP-Ribose and Induce Non-apoptotic Cell Death. *iScience* **15**, 452-466 (2019).
11. R. Aarhus, R. M. Graeff, D. M. Dickey, T. F. Walseth, H. C. Lee, ADP-ribosyl cyclase and CD38 catalyze the synthesis of a calcium-mobilizing metabolite from NADP. *J Biol Chem* **270**, 30327-30333 (1995).
12. Y. Jiang *et al.*, The NAD(+)-mediated self-inhibition mechanism of pro-neurodegenerative SARM1. *Nature* **588**, 658-663 (2020).
13. M. P. Coleman, A. Hoke, Programmed axon degeneration: from mouse to mechanism to medicine. *Nat Rev Neurosci* **21**, 183-196 (2020).
14. W. H. Li *et al.*, Permeant fluorescent probes visualize the activation of SARM1 and uncover an anti-neurodegenerative drug candidate. *Elife* **10** (2021).
15. Y. Shi *et al.*, Structural basis of SARM1 activation, substrate recognition, and inhibition by small molecules. *Mol Cell* **82**, 1643-1659 e1610 (2022).
16. M. Bratkowski *et al.*, Uncompetitive, adduct-forming SARM1 inhibitors are neuroprotective in preclinical models of nerve injury and disease. *Neuron* **110**, 3711-3726 e3716 (2022).
17. Y. Hao *et al.*, Degeneration of Injured Axons and Dendrites Requires Restraint of a Protective JNK Signaling Pathway by the Transmembrane Protein Raw. *J Neurosci* **39**, 8457-8470 (2019).
18. T. J. Waller, C. A. Collins, Opposing roles of Fos, Raw, and SARM1 in the regulation of axonal degeneration and synaptic structure. *Front Cell Neurosci* **17**, 1283995 (2023).
19. K. L. Bates, M. Higley, A. Letsou, Raw mediates antagonism of AP-1 activity in Drosophila.

*Genetics* **178**, 1989-2002 (2008).

20. D. Luong, L. Perez, J. C. Jemc, Identification of raw as a regulator of glial development. *PLoS One* **13**, e0198161 (2018).
21. J. Zhou, B. A. Edgar, M. Boutros, ATF3 acts as a rheostat to control JNK signalling during intestinal regeneration. *Nat Commun* **8**, 14289 (2017).
22. M. Varadi *et al.*, AlphaFold Protein Structure Database in 2024: providing structure coverage for over 214 million protein sequences. *Nucleic Acids Res* **52**, D368-D375 (2024).
23. L. A. O'Neill, A. G. Bowie, The family of five: TIR-domain-containing adaptors in Toll-like receptor signalling. *Nat Rev Immunol* **7**, 353-364 (2007).
24. S. Pande, X. Yang, R. Friesel, Interleukin-17 receptor D (Sef) is a multi-functional regulator of cell signaling. *Cell Commun Signal* **19**, 6 (2021).
25. A. M. Burroughs, D. Zhang, D. E. Schaffer, L. M. Iyer, L. Aravind, Comparative genomic analyses reveal a vast, novel network of nucleotide-centric systems in biological conflicts, immunity and signaling. *Nucleic Acids Res* **43**, 10633-10654 (2015).
26. I. Schneider, Cell lines derived from late embryonic stages of Drosophila melanogaster. *J Embryol Exp Morphol* **27**, 353-365 (1972).
27. R. Graeff, H. C. Lee, A novel cycling assay for cellular cADP-ribose with nanomolar sensitivity. *Biochem J* **361**, 379-384 (2002).
28. H. C. Lee, T. Walseth, G. T. Bratt, R. N. Hayes, D. Clapper, Structural determination of a cyclic metabolite of NAD+ with intracellular Ca2+-mobilizing activity. *J. Biol. Chem.* **264**, 1608-1615 (1989).
29. M. Howard *et al.*, Formation and hydrolysis of cyclic ADP-ribose catalyzed by lymphocyte antigen CD38. *Science* **262**, 1056-1059 (1993).
30. Q. Liu *et al.*, Crystal structure of human CD38 extracellular domain. *Structure* **13**, 1331-1339 (2005).
31. G. S. Prasad *et al.*, Crystal structure of Aplysia ADP ribosyl cyclase, a homologue of the bifunctional ectozyme CD38. *Nat Struct Biol* **3**, 957-964 (1996).
32. J. Abramson *et al.*, Accurate structure prediction of biomolecular interactions with AlphaFold 3. *Nature* **630**, 493-500 (2024).
33. Y. N. Hou *et al.*, A conformation-specific nanobody targeting the nicotinamide mononucleotide-activated state of SARM1. *Nat Commun* **13**, 7898 (2022).
34. K. Tobiume *et al.*, ASK1 is required for sustained activations of JNK/p38 MAP kinases and apoptosis. *EMBO Rep* **2**, 222-228 (2001).
35. Y. Chen *et al.*, Aggresome formation promotes ASK1/JNK signaling activation and stemness maintenance in ovarian cancer. *Nat Commun* **15**, 1321 (2024).
36. C. L. Byars, K. L. Bates, A. Letsou, The dorsal-open group gene raw is required for restricted DJNK signaling during closure. *Development* **126**, 4913-4923 (1999).
37. E. J. Brace *et al.*, Distinct developmental and degenerative functions of SARM1 require NAD+ hydrolase activity. *PLoS Genet* **18**, e1010246 (2022).
38. K. A. Herrmann *et al.*, Divergent signaling requirements of dSARM in injury-induced degeneration and developmental glial phagocytosis. *PLoS Genet* **18**, e1010257 (2022).
39. M. Uhlirova, D. Bohmann, JNK- and Fos-regulated Mmp1 expression cooperates with Ras to induce invasive tumors in Drosophila. *EMBO J* **25**, 5294-5304 (2006).
40. T. F. Walseth, H. C. Lee, Synthesis and characterization of antagonists of cyclic-ADP-

ribose-induced Ca2+ release. *Biochim Biophys Acta* **1178**, 235-242 (1993).

41. A. M. Evans, On a Magical Mystery Tour with 8-Bromo-Cyclic ADP-Ribose: From All-or-None Block to Nanojunctions and the Cell-Wide Web. *Molecules* **25** (2020).
42. K. Arora *et al.*, The Drosophila schnurri gene acts in the Dpp/TGF beta signaling pathway and encodes a transcription factor homologous to the human MBP family. *Cell* **81**, 781-790 (1995).
43. J. Jack, G. Myette, The genes raw and ribbon are required for proper shape of tubular epithelial tissues in Drosophila. *Genetics* **147**, 243-253 (1997).
44. S. Noselli, F. Agnes, Roles of the JNK signaling pathway in Drosophila morphogenesis. *Curr Opin Genet Dev* **9**, 466-472 (1999).
45. K. A. Guss *et al.*, Expression and function of scalloped during Drosophila development. *Dev Dyn* **242**, 874-885 (2013).
46. V. L. Czech, L. C. O'Connor, B. Philippon, E. Norman, A. B. Byrne, TIR-1/SARM1 inhibits axon regeneration and promotes axon degeneration. *Elife* **12** (2023).
47. S. L. Bauer Huang *et al.*, Left-right olfactory asymmetry results from antagonistic functions of voltage-activated calcium channels and the Raw repeat protein OLRN-1 in C. elegans. *Neural Dev* **2**, 24 (2007).
48. H. C. Lee, Y. J. Zhao, Resolving the topological enigma in Ca(2+) signaling by cyclic ADP-ribose and NAADP. *J Biol Chem* **294**, 19831-19843 (2019).
49. H. Yu *et al.*, Activation of a helper NLR by plant and bacterial TIR immune signaling. *Science* 10.1126/science.adr3150, eadr3150 (2024).
50. A. M. Bayless *et al.*, Plant and prokaryotic TIR domains generate distinct cyclic ADPR NADase products. *Science advances* **9**, eade8487 (2023).
51. G. Ofir *et al.*, Antiviral activity of bacterial TIR domains via immune signalling molecules. *Nature* **600**, 116-120 (2021).
52. S. Eastman *et al.*, A phytobacterial TIR domain effector manipulates NAD(+) to promote virulence. *The New phytologist* 10.1111/nph.17805 (2021).
53. G. Tauriello *et al.*, ModelArchive: A Deposition Database for Computational Macromolecular Structural Models. *J Mol Biol* **437**, 168996 (2025).

# Figures

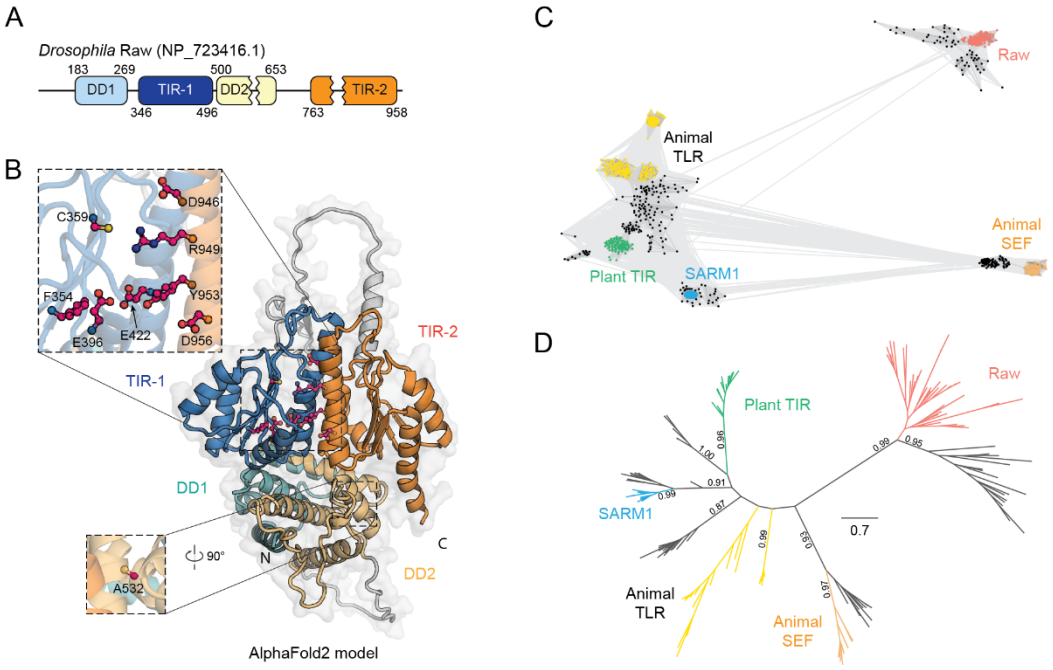


**Figure 1. Raw defines a distinct family of TIR domain proteins.**
(**A**) Schematic of Raw domain composition (NP_723416.1): DD1 in light blue, TIR1 in dark blue, DD2 in yellow, and C-terminal TIR2 in orange, with annotated domain boundaries. (**B**) AlphaFold2-predicted structural model of Raw, colored according to (A). Predicted catalytic residues from both TIR1 and TIR2 domains are shown in ball-and-stick format (C, pink; N, blue; O, red; S, orange). (**C**) Sequence-similarity network of the Raw-TIR family (light red) compared with other TIR families: animal TLR-TIR (yellow), animal SEF-TIR (orange), SARM1-TIR (sky blue), plant NLR-TIR (green), and bacterial homologs (black). Each node represents a protein; edges indicate high-scoring segment pairs from all-against-all BLASTP searches (BLOSUM62, e-value < $1 \times 10^{-4}$). (**D**) Unrooted Maximum Likelihood phylogenetic tree of Raw-TIR and other TIR families. Families are colored as in (C); bootstrap support from 100 replicates is shown for major branches only.

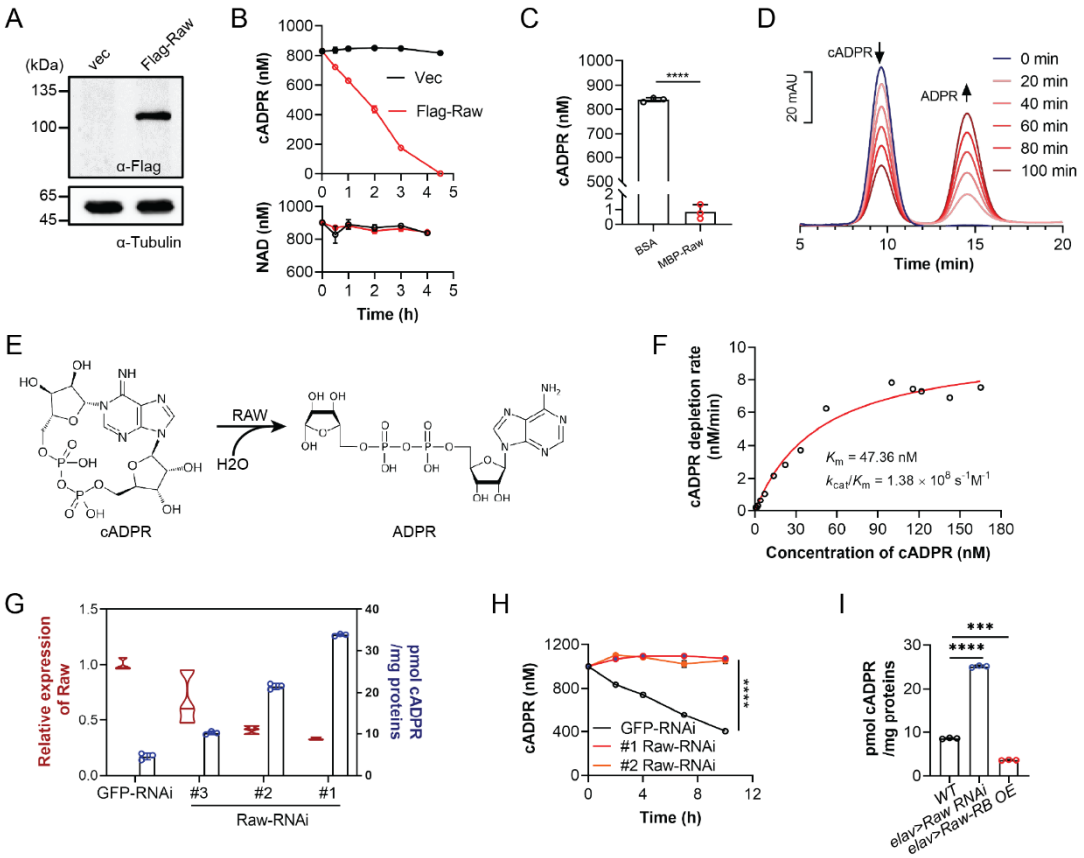


**Figure 2. Characterization of Raw as a novel cADPR hydrolase.**

(**A**) Western blot of Flag-Raw in S2 cells; α-tubulin as loading control. (**B**) Enzymatic activity of Raw cell lysate with NAD or cADPR; empty-vector lysate as control. (**C**) Activity of recombinant MBP-Raw with cADPR; BSA as negative control. (**D**) HPLC assay of MBP-Raw activity (100 μM cADPR, 50 μg/ml enzyme). (**E**) Chemical equation for Raw-catalyzed cADPR hydrolysis. (**F**) Michaelis–Menten plot for Raw-catalyzed cADPR hydrolysis (*K*m, *k*cat). (**G**) Inverse correlation between Raw mRNA (qRT-PCR) and cADPR (cycling assay) in S2 cells treated with three Raw dsRNAs; GFP RNAi as control. (**H**) cADPR degradation by cell lysates (50 μg/ml) from (G). (**I**) Inverse correlation between Raw expression and cADPR levels in *Drosophila* heads from *elav*-Gal4 crosses with UAS-*Raw* RNAi or UAS-*Raw* RB OE lines.

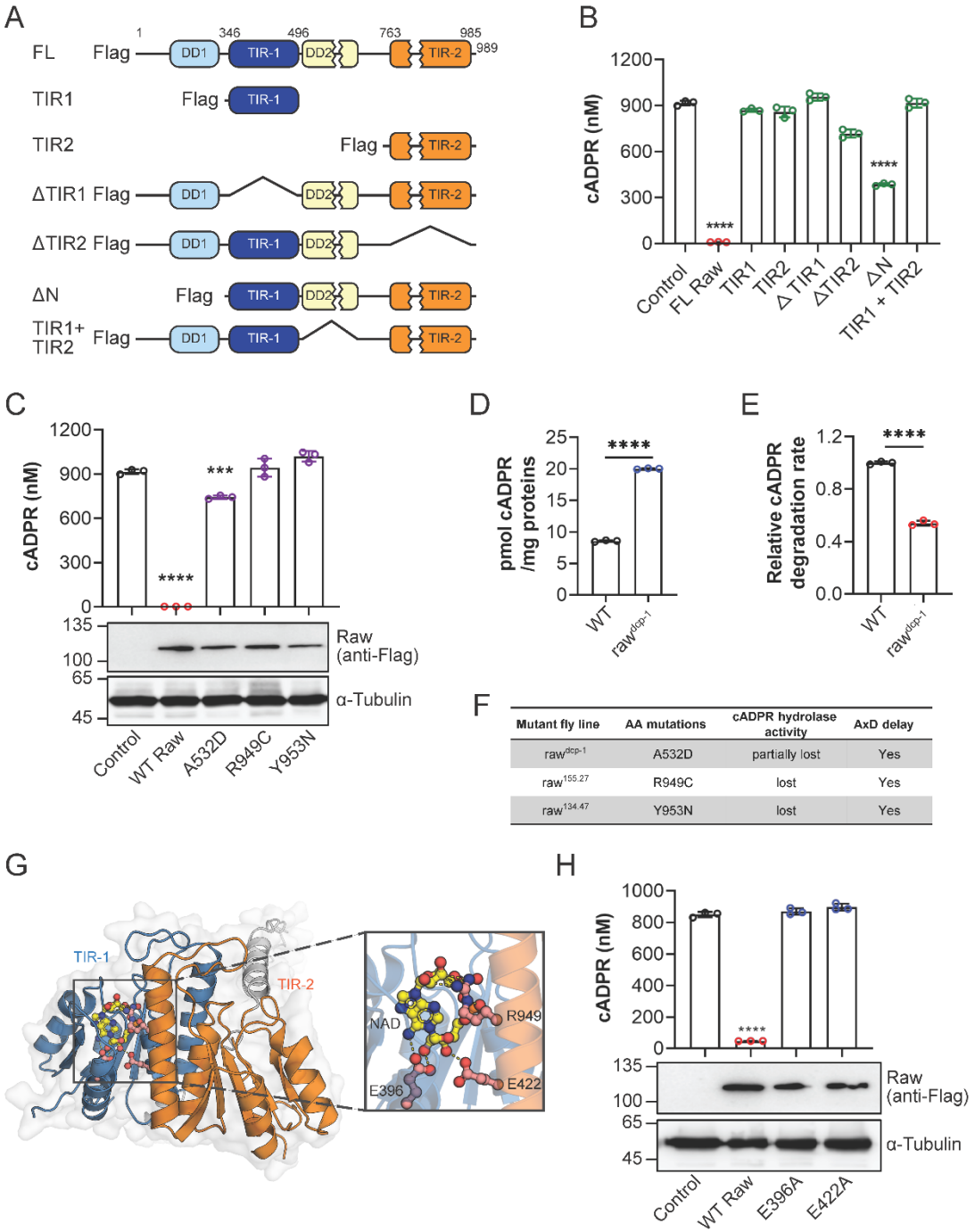


| Mutant fly line | AA mutations | cADPR hydrolase activity | AxD delay |
|---|---|---|---|
| raw$^{dcp-1}$ | A532D | partially lost | Yes |
| raw$^{155.27}$ | R949C | lost | Yes |
| raw$^{134.47}$ | Y953N | lost | Yes |

**Figure 3. Key domains and residues required for Raw enzymatic activity.**
(**A**) Schematic of Raw truncation constructs; FL, full length. (**B**) Enzymatic activity of the Raw mutants. (**C**) Activity of Raw mutants as in (B); protein levels assessed by Western blot (sizes in kDa). (**D**) cADPR levels in heads of 2-week-old WT and mutant flies (cycling assay). (**E**) Raw expression in heads of WT and mutant flies (qRT-PCR) and activity assays with equal Raw protein amounts and 1 μM cADPR; cADPR consumption rate plotted. (**F**) Correlation between cADPR hydrolase activity and AxD delay phenotype. (**G**) AlphaFold3-predicted Raw-cADPR interaction. (**H**) Activity of additional Raw mutants as in (C).

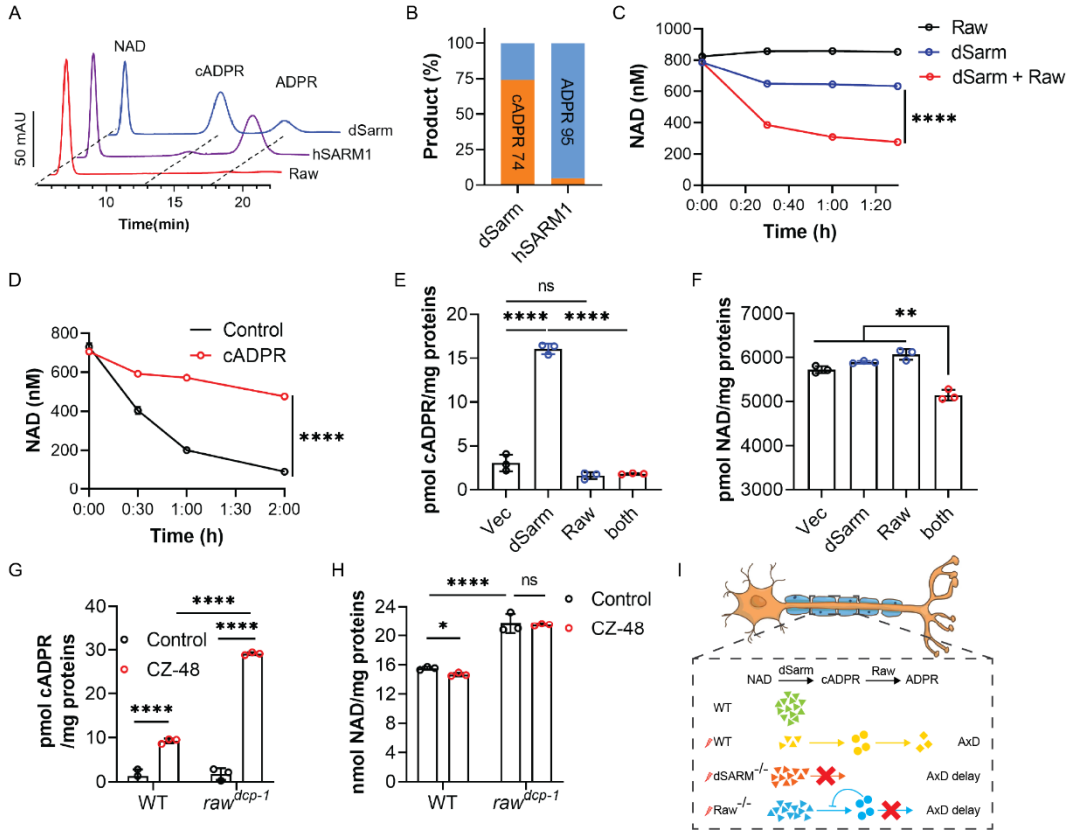


**Figure 4. Synergistic role of Raw and dSarm in NAD depletion during axon degeneration.**

(**A**) HPLC assay of recombinant dSarm, hSarm1, or Raw (50 μg/ml) incubated with 100 μM NAD for 2 h. (**B**) Percentage of products formed in (A). (**C**) Time course of NAD depletion by dSarm and Raw (5 μg/ml), alone or combined; NAD measured every 30 min (cycling assay). (**D**) Effect of 800 nM cADPR on NAD consumption by dSarm (10 μg/ml, 800 nM NAD). (**E-F**) NAD and cADPR levels in S2 cells expressing dSarm and/or Raw; empty-vector transfection as control. (**G-H**) cADPR and NAD levels in heads of WT and *raw*$^{dcp-1}$ flies after 30 min with 100 μM CZ-48. (**I**) Proposed model for the synergistic mechanism of dSarm and Raw in NAD depletion.

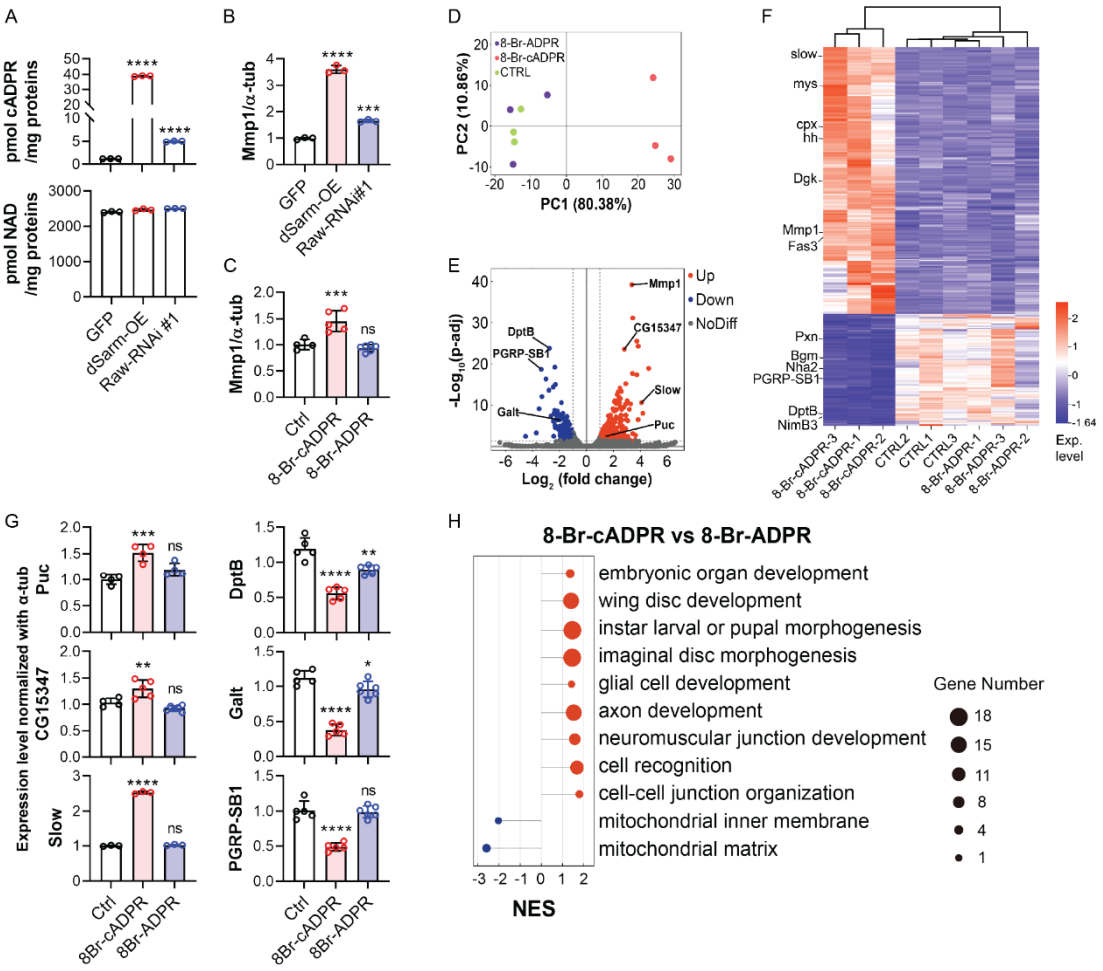


**Figure 5. cADPR activates the kinase pathway related to organ development.** (**A**) cADPR and NAD levels in S2 cells with dSarm overexpression (*dSarm*-OE) or Raw knockdown; measured by cycling assay. (**B-C**) *Mmp1* expression in dSarm-OE and Raw RNAi S2 cells (B), or S2 cells treated with 50 μM 8-Br-cADPR or 8-Br-ADPR for 24 h (C); measured by qRT-PCR. (**D**) PCA of vehicle control (green), 8-Br-ADPR control (purple), and 8-Br-cADPR-treated samples. (**E**) Volcano plot of DEGs after treatment of 8-Br-cADPR vs 8-Br-ADPR; $P < 0.05$, $|\log_2 FC| > 1$; upregulated (red), downregulated (blue), non-significant (gray); qRT-PCR-validated genes labeled. (**F**) Hierarchical heatmap of top 319 DEGs; columns = samples, rows = genes; scale bar shows relative expression. (**G**) qRT-PCR validation of gene expression changes after treatments as in (C). (**H**) Top enriched GO pathways from GSEA; bubble size = number of DEGs, color = upregulated (red) or downregulated (blue); FDR < 0.25, NES > 1.

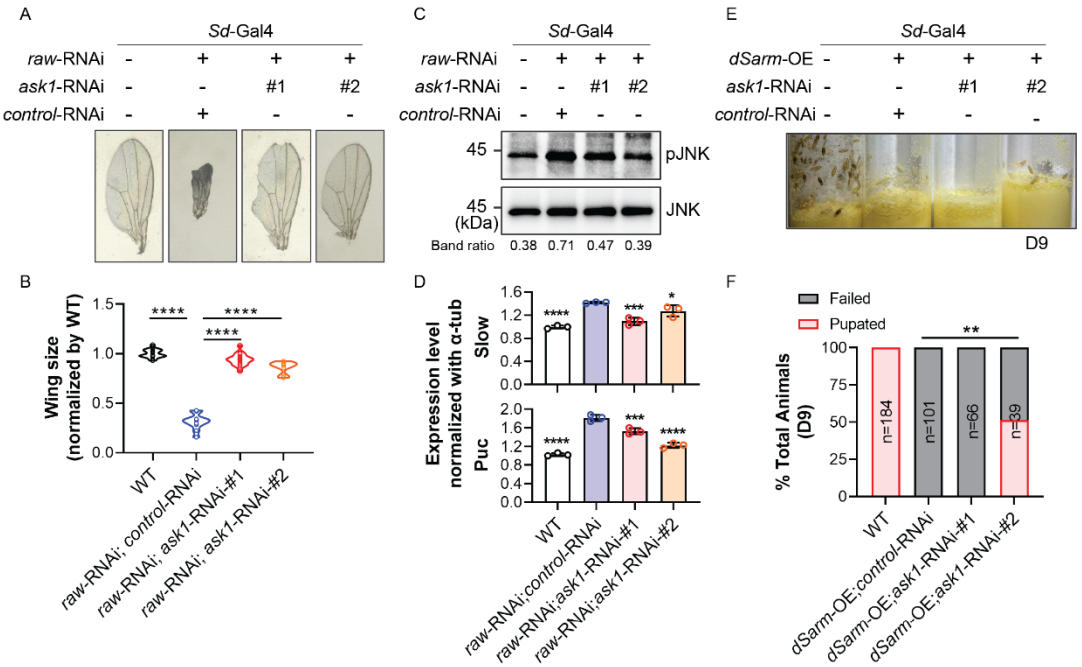


**Figure 6. Raw/cADPR signaling in wing development.**

(**A**) Adult wing micrographs showing effects of *raw* RNAi and *ask*1 RNAi; *Sd*-Gal4 driving *raw* RNAi in the Sd domain with co-expression of *ask1* RNAi (#1, #2) or *mCherry* RNAi (control). (**B**) Wing size quantification; areas measured by ImageJ, expressed as ratio to WT wings. (**C**) Western blot of phosphorylated JNK (pJNK) and total JNK in wing discs from third-instar larvae: *Sd*>WT, *Sd*>*raw*-RNAi;*control*-RNAi, and *Sd*>*raw*-RNAi;*ask1*-RNAi. (**D**) qRT-PCR of *Puc* and *Slow* transcripts in wing discs from third-instar larvae, with genetic background as (C); normalized to *α-tubulin*. (**E**) Developmental progression of flies on day 9 after egg laying: *Sd*>WT, *Sd*>*dSarm*-OE;*control*-RNAi, and *Sd*>*dSarm*-OE;*ask1*-RNAi. (**F**) Quantification of pupae on day 9 in flies as (E).

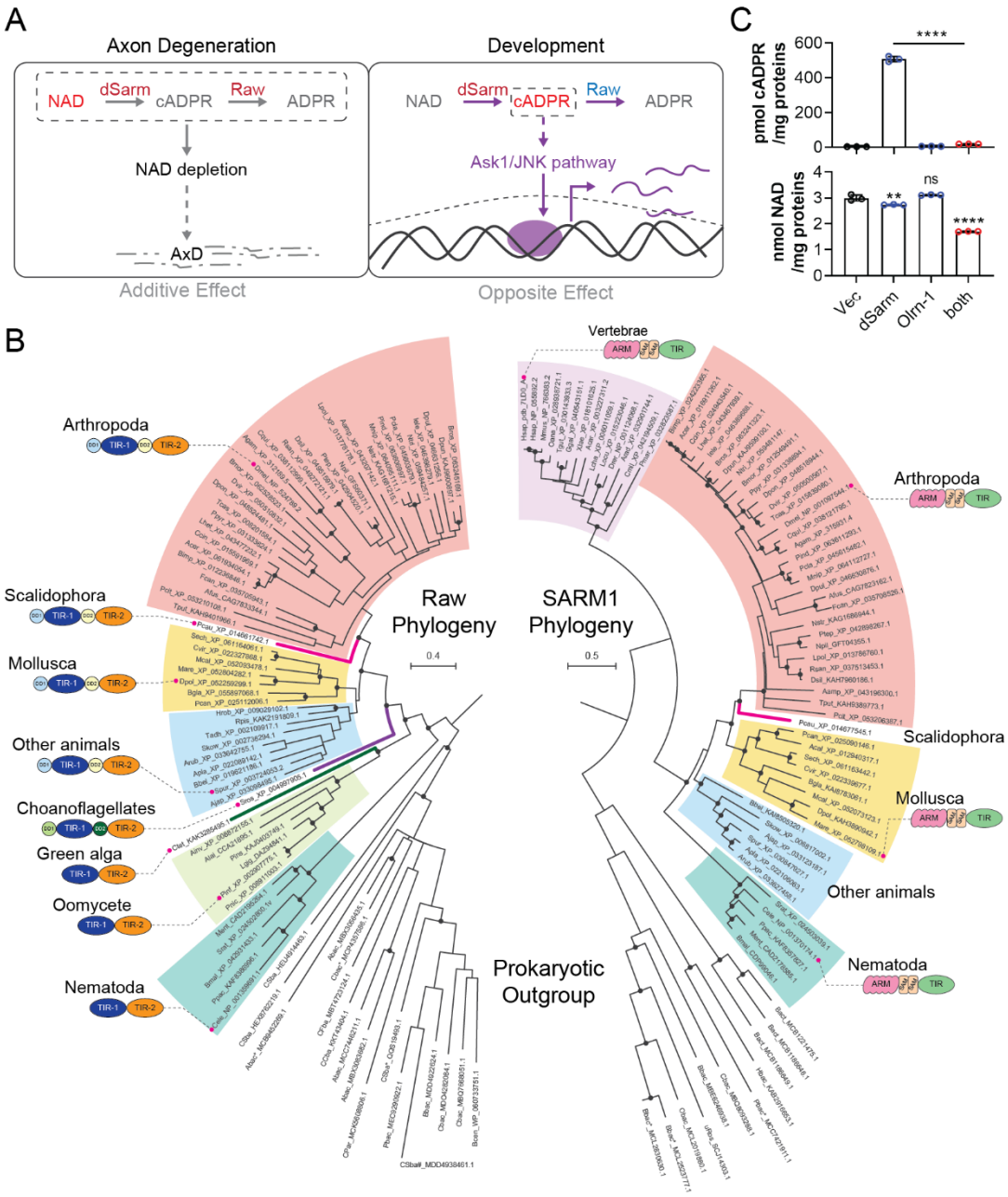


**Figure 7. Molecular interplay and co-evolution between Raw and SARM1.**
(**A**) Model of dSarm-Raw interplay in axon degeneration and organ development. (**B**) Phylogenetic trees of TIR domains from Raw (left) and SARM1 (right), inferred using Maximum Likelihood (JTT model, MEGA7); highest log-likelihood trees shown. Bootstrap values >75% are marked with black dots. Sequences are labeled by species abbreviation and NCBI accession number. Clades are color-coded: vertebrates (light purple), Arthropoda (red), Mollusca (yellow), other animals (light blue), Oomycete (light green), Nematoda (teal), Scalidophora (hot pink), Choanoflagellates (purple), green algae (green), and prokaryotes (black, no background). Representative domain architectures for major clades are shown alongside the trees. (**C**) Enzymatic activity of Olrn-1 in HEK-293T cells expressing Flag-dSarm and/or Olrn-1; cADPR (upper) and NAD (lower) measured by cycling assay. Empty-vector transfection as control.